Proceedings of the ASME 2020
International Design Engineering Technical Conferences
and Computers and Information in Engineering Conference
IDETC/CIE2020
August 16-19, 2020, Hilton, St. Louis, MO, USA

IDETC2020-22120

THREE-DIMENSIONAL SYMMETRIC MAXIMUM WEIGHT LIFTING PREDICTION

Rahid Zaman, Yujiang Xiang¹,
Mechanical and Aerospace Engineering
Oklahoma State University
Stillwater, Oklahoma 74078, USA

Jazmin Cruz, James Yang
Department of Mechanical Engineering
Texas Tech University
Lubbock, Texas 79409, USA

ABSTRACT

Lifting heavy weight is one of the main reasons for manual material handling related injuries which can be mitigated by determining the limiting lifting weight of a person. In this study, a 40 degrees of freedom (DOFs) spatial skeletal model was employed to predict the symmetric maximum weight lifting motion. The lifting problem was formulated as a multi-objective optimization (MOO) problem to minimize the dynamic effort and maximize the box weight. An inverse-dynamics-based optimization approach was used to determine the optimal lifting motion and the maximum lifting weight considering dynamic joint strength. The predicted lifting motion, ground reaction forces (GRFs), and maximum box weight were shown to match well with the experimental results. It was found that for the three-dimensional (3D) symmetric lifting the left and right GRFs were not same.

Keywords: Lifting, Symmetric lifting, Maximum weight lifting, Dynamic joint strength, Multi-objective optimization.

1. INTRODUCTION

Despite the advancement in robotics and automation fields, manual material handling (MMH) related injuries like hyperextension and occupational hazards are the most common cause of disability [1]. Low back pain from hyperextension is the leading cause for visits to orthopedic surgeons and neurosurgeons and the second common cause for visits to physicians [2, 3]. The direct costs of MMH related injuries are over \$13 billion in 2016 [4], whereas the indirect costs are more than \$100 billion per year [5]. Lifting is one of the most common causes for Musculoskeletal Disorders (MSDs) like low back pain [6, 7]. Therefore, it is necessary to identify the maximum lifting weight for a person as well as the reasons behind lifting work-related injuries. In practice, it is difficult to find the best lifting motion and true maximum lifting weight through laboratory experiment as it is risky for the participants [8]. An optimization-

based biomechanical model can assist in finding the best lifting motion as well as the maximum lifting weight.

Over the past decades, many researchers have been working on human biomechanical modeling. However, only a few researchers have worked on lifting motion prediction. Initially, some researchers worked on the two-dimensional (2D) model. For example, based on the NIOSH (National Institute of Occupational Safety and Health) lifting equation, a static and 2D biomechanical model was proposed to estimate the strength needed for a specific MMH task [9]. In another study, a 5-link sagittal model was used to predict the optimum lifting motion using space-time optimization [10]. Another 5-link 2D model was introduced to predict the lifting motion based on the static joint strength [11].

But, dynamic joint strength is required to predict the maximum lifting weight in the optimization formulation. The dynamic joint strength is a function of joint angle and angular velocity [12, 13, 14, 15]. In Gundogdu et al. [16], a 2D dynamic-joint-strength-based model was presented to predict the optimal lifting motion using generic algorithm. Another 2D human model was proposed to predict the symmetric maximum weight lifting motion based on the dynamic joint strength [17, 18]. In Sreenivasa et al. [19], a 12-DOF 2D model was used to study the influence of hip and lumber flexibility during lifting motion considering the dynamic joint strength.

Optimization-based approach is an effective way to solve a redundant system. As multi-link human model is a highly redundant system, optimization-based approach is a preferred tool to find the optimal lifting motion. However, for optimization-based approaches, choosing the objective functions play a vital role in predicting the lifting motion accurately. A 2D model was developed based on the MOO to predict the lifting motion [18]. The MOO approach results in an 18.9% reduction in the overall root mean square (RMS) joint angle error when compared to the single objective optimization based lifting motion prediction [20]. However, 2D models do not give the total scenario of a lifting motion, as they do not consider lifting

© 2020 by ASME

¹ Corresponding author: yujiang.xiang@okstate.edu

weight differences on two sides of the sagittal plane of a human body. A 3D model can give more insight into the lifting motion. A 3D biomechanical model was proposed, where lumbar forces were considered as the objective function to study the effect of lumbar torque limit during lifting [21]. In another study, a 3D skeletal model was used with four objective functions, which had the functionality to analyze the lifting motion for each objective function separately [22]. MOO was also incorporated in a 3D model to predict the lifting motion more accurately [23, 24].

On the other hand, only a few studies were conducted to predict the maximum lifting weight considering the dynamic strength [17, 25]. In this study, a 40-DOF 3D model is used to predict the symmetric lifting motion, lifting time and maximum lifting weight using an inverse-dynamics-based MOO approach. The predicted results are validated by comparing the predicted kinematics and kinetics data with the experimental data.

2. 3D SKELETON MODEL AND PREDICTIVE SIMULATION

The 3D skeletal model consists of 40 DOFs, which are expressed as $\mathbf{q} = [z_1 \ z_2 \ z_3 \ \ z_{40}]$, and the kinematic chains are connected using well developed Denavit-Hartenberg (DH) representations [26]. The model consists of one virtual branch and five physical branches. The virtual branch contains three rotational DOFs and three translational DOFs, which allows the model to move in the global space. On the other hand, physical branches are the spine, right arm, left arm, right leg and left leg. There are six DOFs for the spine, seven DOFs for each arm, and seven DOFs for each leg. Each arm consists of three segments: upper arm, forearm and hand. Each leg consists of four segments: thigh, shank, rear foot and forefoot.

The anthropometric data of the model are generated in Visual 3D® (C-Motion, Inc., Germantown, MD, USA) software using experimentally measured height, weight and stature data. The dynamic joint strength of the model is retrieved from the symmetric maximum weight lifting experiment [17].

The general equations of motion of this biomechanical model are based on the recursive Lagrangian formulation, and can be expressed in matrix form, which contains forward recursive kinematics and backward recursive dynamics [27].

2.1 Forward Recursive Kinematics

$$\mathbf{A}_i = \mathbf{A}_{i-1} \mathbf{T}_i, \tag{1}$$

$$\mathbf{B}_{i} = \dot{\mathbf{A}}_{i} = \mathbf{B}_{i-1} \mathbf{T}_{i} + \mathbf{A}_{i-1} \frac{\partial \mathbf{T}_{i}}{\partial q_{i}} \dot{q}_{i}, \tag{2}$$

$$\mathbf{C}_i = \dot{\mathbf{B}}_i = \mathbf{C}_{i-1}\mathbf{T}_i + 2\mathbf{B}_{i-1}\frac{\partial \mathbf{T}_i}{\partial q_i}\dot{q}_i + \mathbf{A}_{i-1}\frac{\partial^2 \mathbf{T}_i}{\partial q_i^2}\dot{q}_i^2 + \mathbf{A}_{i-1}\frac{\partial \mathbf{T}_i}{\partial q_i}\ddot{q}_i(3)$$

where q_i is the joint angle variable, \mathbf{T}_i is the 4×4 DH link transformation matrix from the (i-1)th link frame to the ith link frame, \mathbf{A}_i , \mathbf{B}_i , \mathbf{C}_i are the global recursive kinematics position, velocity, and acceleration matrices, respectively, and $\mathbf{A}_0 = [\mathbf{I}]$, $\mathbf{B}_0 = \mathbf{C}_0 = [\mathbf{0}]$.

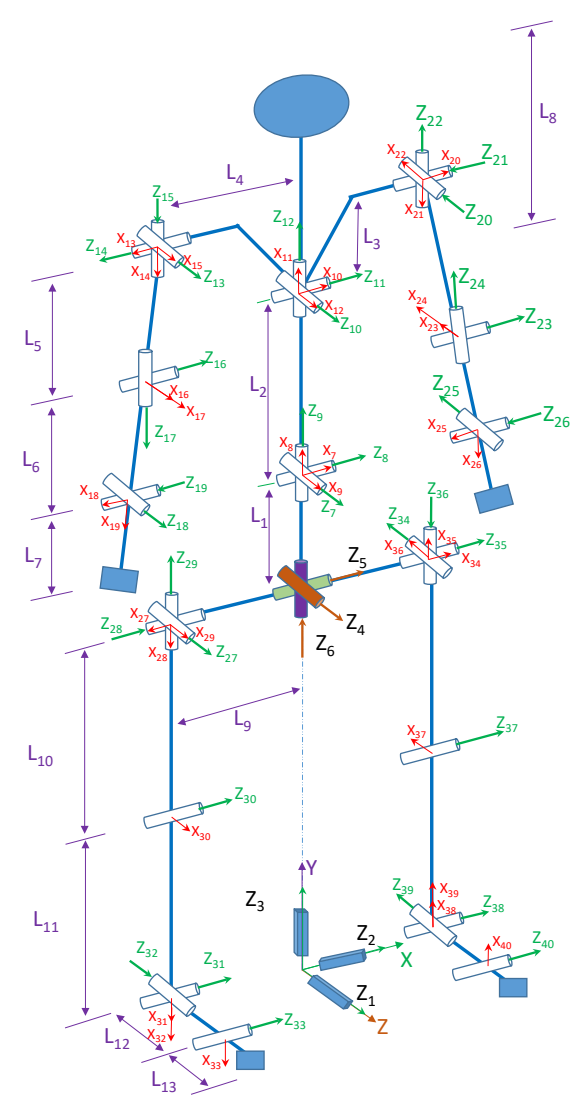


FIGURE 1: THREE-DIMENSIONAL SKELETAL MODEL

2.2 Backward Recursive Dynamics

$$\tau_{i} = \operatorname{tr}\left(\frac{\partial \mathbf{A}_{i}}{\partial \mathbf{q}_{i}} \mathbf{D}_{i}\right) - \mathbf{g}^{\mathrm{T}} \frac{\partial \mathbf{A}_{i}}{\partial q_{i}} \mathbf{E}_{i} - \mathbf{f}_{k}^{\mathrm{T}} \frac{\partial \mathbf{A}_{i}}{\partial q_{i}} \mathbf{F}_{i} - \mathbf{G}_{i}^{\mathrm{T}} \mathbf{A}_{i-1} \mathbf{z}_{0}, \tag{4}$$

$$\mathbf{D}_i = \mathbf{I}_i \mathbf{C}_i^{\mathrm{T}} + \mathbf{T}_{i+1} \mathbf{D}_{i+1}, \tag{5}$$

$$\mathbf{E}_i = m_i \mathbf{r}_i + \mathbf{T}_{i+1} \mathbf{E}_{i+1},\tag{6}$$

$$\mathbf{F}_{i} = \mathbf{r}_{k} \delta_{ik} + \mathbf{T}_{i+1} \mathbf{F}_{i+1}, \tag{7}$$

$$\mathbf{G}_{i} = \mathbf{h}_{k} \delta_{ik} + \mathbf{G}_{i+1}, \tag{8}$$

where $tr(\cdot)$ is the trace of a matrix, \mathbf{I}_i is the inertia matrix for link i, \mathbf{D}_i is the recursive inertia and Coriolis matrix, \mathbf{E}_i is the recursive vector for gravity torque calculation, \mathbf{F}_i is the recursive

vector for external force torque calculation, \mathbf{G}_i is the recursive vector for external moment torque calculation, \mathbf{g} is the gravity vector, m_i is the mass of link i, \mathbf{r}_i is the center of mass of link i, $\mathbf{f}_k = [f_{kx} \quad f_{ky} \quad f_{kz} \quad 0]^{\mathrm{T}}$ is the external force applied on link k, \mathbf{r}_k is the position of the external force in the local frame k, $\mathbf{h}_k = [h_x \quad h_y \quad h_z \quad 0]^{\mathrm{T}}$ is the external moment applied on link k, $\mathbf{z}_0 = [0 \quad 0 \quad 1 \quad 0]^{\mathrm{T}}$ is for a revolute joint, $\mathbf{z}_0 = [0 \quad 0 \quad 0]^{\mathrm{T}}$ is for a prismatic joint, δ_{ik} is Kronecker delta, and the starting conditions are $\mathbf{D}_{n+1} = [\mathbf{0}]$, $\mathbf{E}_{n+1} = \mathbf{F}_{n+1} = \mathbf{G}_{n+1} = [\mathbf{0}]$.

The 40-DOF spatial model is a highly redundant system. The lifting task is formulated as a nonlinear programming problem (NLP) and is solved by an inverse-dynamics-based optimization method. The design variables (\mathbf{x}) include control points (\mathbf{c}) of cubic B-spline curves of joint angles, box weight (W), and total lifting time (T) as $\mathbf{x} = [\mathbf{c}^T \ W \ T]^T$. The MOO is used to minimize the dynamic effort and maximize the lifting weight. Finally, the combined objective function is defined as [18].

$$J = w_1 N \left[\int_0^T \sum_{i=7}^n \left(\frac{\tau_i(x,t)}{\tau_i^U - \tau_i^L} \right)^2 dt \right] - w_2 N [\log(W + 10)], \tag{9}$$

where N[·] is the normalization function, n is the number of DOFs, τ_i^L and τ_i^U are the ith lower and upper dynamic joint torque limits, respectively, w_1 and w_2 are weighting coefficients for the two normalized objective functions where $w_1 = 0.15$ and $w_2 = 0.85$ [18].

There are two types of constraints imposed on the lifting motion: time-dependent constraints and time-independent constraints.

2.3 Time-dependent Constraints

(1) Joint angle limits imposed in the formulation are from experiments and can be expressed as:

$$\mathbf{q}^{L} \le \mathbf{q}(\mathbf{x}, t) \le \mathbf{q}^{U},\tag{10}$$

where \mathbf{q}^L and \mathbf{q}^U represent the lower and upper limits on the joint angles respectively.

(2) Dynamic joint torque is a function of joint angle (q), angular velocity (v), strength percentile (z_{score}) and time (t) [17]. The dynamic joint strength imposed in this formulation can be expressed as:

$$\tau_i^L(q_i, v_i, z_{score}, t) \le \tau_i \le \tau_i^U(q_i, v_i, z_{score}, t), \tag{11}$$

where τ_i is the simulated joint torque for the *i*th joint, τ_i^U is the upper torque value for the *i*th joint in positive q_i direction and τ_i^L is the lower torque value for the *i*th joint in negative q_i direction. Details about dynamic joint torque constraint can be found in Xiang et al. [18].

(3) Foot-contacting position constraint is imposed to keep the skeleton model on the ground and can be expressed as:

$$\mathbf{p}_{feet}(\mathbf{x},t) = \mathbf{p}_{s},\tag{12}$$

where \mathbf{p}_{feet} are the calculated feet positions, \mathbf{p}_{s} are specified feet ground contacting positions.

(4) Dynamic balance constraint prevents the skeletal model from falling and helps to keep the body stable. This constraint is imposed by enforcing the location of zero-moment-point (ZMP), $\mathbf{p}_{ZMP}(\mathbf{x},t)$, inside the foot support region (FSR) [28, 29] and is expressed as:

$$\mathbf{p}_{ZMP}(\mathbf{x},t) \in FSR. \tag{13}$$

(5) Box-collision avoidance is imposed in this formulation by filling up the model with spheres on the ankle, shank, knee, thing, hip, lower spine and higher spine to avoid the penetration of box into the body. The constraint is expressed as:

$$d(\mathbf{x},t) \ge r + \frac{dep}{2},\tag{14}$$

where r is the radius of a sphere to represent body thickness, dep is the box depth and d is the distance between the centers of the box and the sphere.

(6) For grasping the box, hand distance constraint is imposed to keep the distance between the two wrists in 3D space equal to box width and is expressed as:

$$\left\|\mathbf{p}_{right_hand}(\mathbf{x},t) - \mathbf{p}_{left_hand}(\mathbf{x},t)\right\|_{2} = wid,$$
 (15)

where \mathbf{p}_{right_hand} and \mathbf{p}_{left_hand} are the right and left hand locations, respectively, and *wid* is the width of the box.

(7) Box-ground parallel constraint is necessary to keep the box parallel to the ground and is imposed by keeping both hand height at same level in 3D space.

$$h_{right\ hand}(\mathbf{x},t) = h_{left\ hand}(\mathbf{x},t), \tag{16}$$

where h_{right_hand} and h_{left_hand} are the right and left hand heights, respectively.

- (8) To distribute the load evenly on both hands, a constraint is imposed to restrict the difference of weight on both hand within 2 N.
- (9) A symmetric lifting motion constraint is applied as the experimental lifting motion was symmetric.

2.4 Time-independent constraints

(1) The initial and final hand (box) locations are given from experiments,

$$\mathbf{p}_{hand}(\mathbf{x},t) = \mathbf{p}_{box}^{s}(t), \qquad t = 0, T$$
 (17)

(2) The whole body will be at rest at the initial and final time points.

$$\dot{\mathbf{q}}(\mathbf{x},t) = \mathbf{0}, \qquad t = 0, T \tag{18}$$

(3) Initial, mid-time, and final key joint angles are given from experimental data.

$$|q_i(\mathbf{x},t) - q_i^E(t)| \le \varepsilon, \qquad t = 0, \frac{\tau}{2}, T$$
(19)

where q_i^E is the experimental joint angle for the *i*th joint including right and left ankle flexion, right and left knee flexion, right and left hip flexion, right and left elbow flexion, spine flexion and rotation, $\varepsilon = 10$ degree at boundaries and $\varepsilon = 5$ degree at mid-time point [8].

(4) Initial, intermediate, and final vertical GRFs are given from experimental data:

$$\left| GRF_{left}(\mathbf{x},t) - GRF_{left}^{E}(t) \right| \le 40, \quad t = 0, \frac{T}{3}, \frac{T}{2}, \frac{2T}{3}, T$$
 (20a)

$$\left| GRF_{right}(\mathbf{x},t) - GRF_{right}^{E}(t) \right| \leq 40, \quad t = 0, \frac{T}{3}, \frac{T}{2}, \frac{2T}{3}, T \quad (20b)$$

where GRF_{left}^{E} , GRF_{right}^{E} are the experimental vertical ground reaction force for left foot and right foot, respectively.

The optimal lifting motion is solved using the sequential quadratic programming (SQP) based optimizer SNOPT [30].

3. EXPERIMENTAL DATA COLLECTION

To ensure the accuracy of the proposed method, motion capture data from a healthy young male adult were collected and compared with the simulation data. The participant signed an informed consent form, and the experimental protocol was approved by the Texas Tech University Institutional Review Board.

Motion data were collected from 42 reflective markers (9 mm, spherical) using a 5-camera Vicon® system (Vicon Motion Systems, Ltd., Oxford, UK) at 100 Hz. Ground reaction forces (GRFs) data were collected using two Kistler® force plates (Kistler, Winterthur, Switzerland) at 2000 Hz.

The maximum lifting weight determined in the experiment is the safe maximum lifting weight, rather than the true maximum weight a subject can lift. To determine the maximum lifting weight, each participant was instructed to lift a box (65 cm \times 35 cm \times 15 cm) up to 1 meter height. The load on the box was incremented by 5 lbs. We stopped once the participant felt that they were uncomfortable with more weight being added. Once the weight was determined, the lifting study was initiated.

The motion capture data and GRFs data were smoothed in Vicon® software using a Butterworth filter with cutoff frequencies of 6 Hz and 25 Hz, respectively.

4. RESULTS AND DISCUSSION

The simulation and experimental data are compared in this study. It took 7.8 minutes for an Intel (R) Xeon (R) E-218G CPU @ 3.80GHz to solve the nonlinear optimization problem using SNOPT. The strength (z_{score}) of the predictive model is 1.05 [21]. The predicted maximum lifting weight on right and left hand are

134.65 N and 132.99 N and the optimal lifting time is 1.3 seconds.

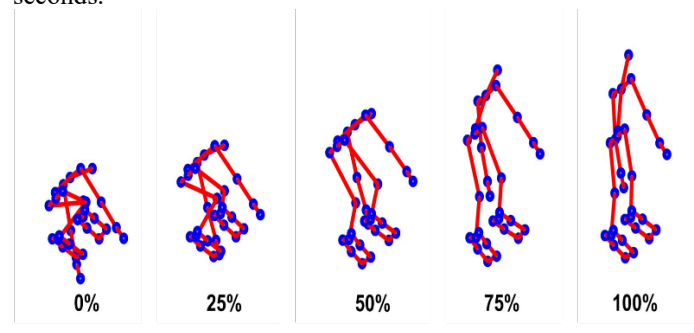
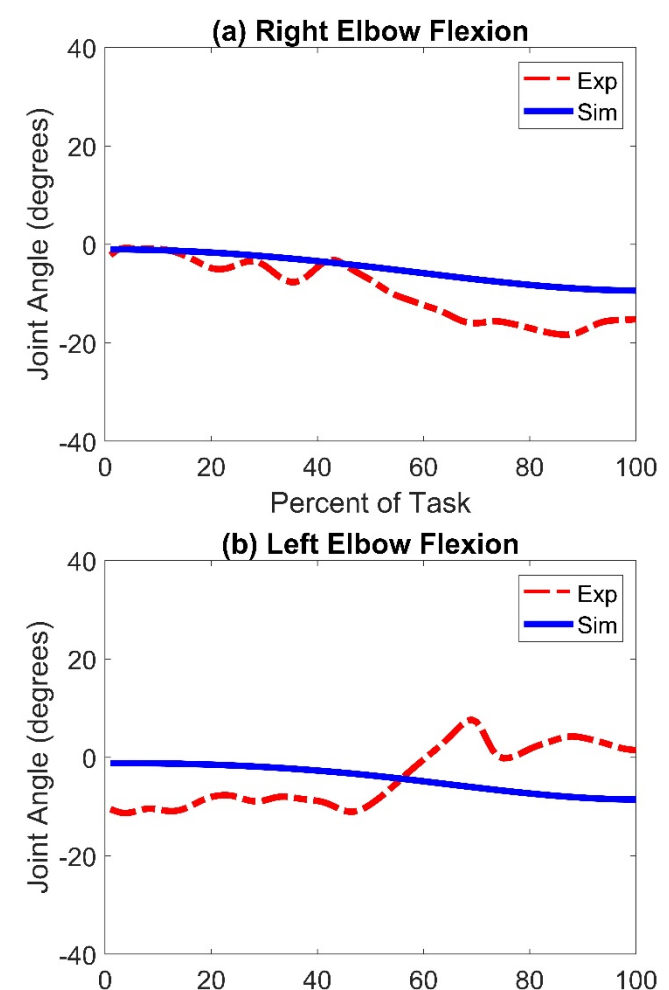
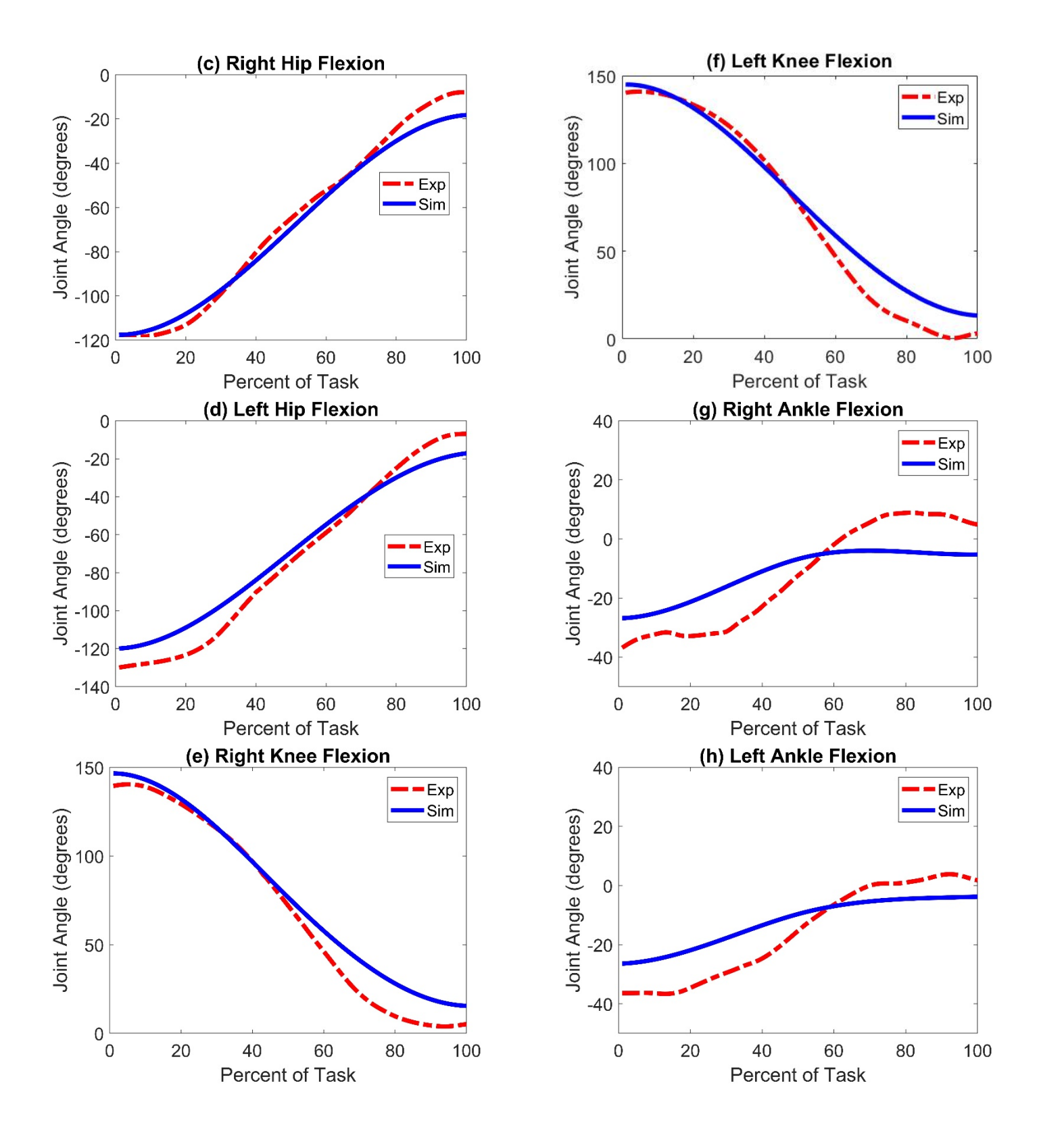


FIGURE 2: THE PREDICTED SYMMETRIC LIFTING MOTION

Figure 2 shows the simulated symmetric lifting motion. Figure 3 shows the joint angle comparisons between the simulation and experimental data. Finally, Figure 4 shows the comparison of GRFs during lifting. The dotted line represents the experimental data and the straight line represents the simulated data.



Percent of Task



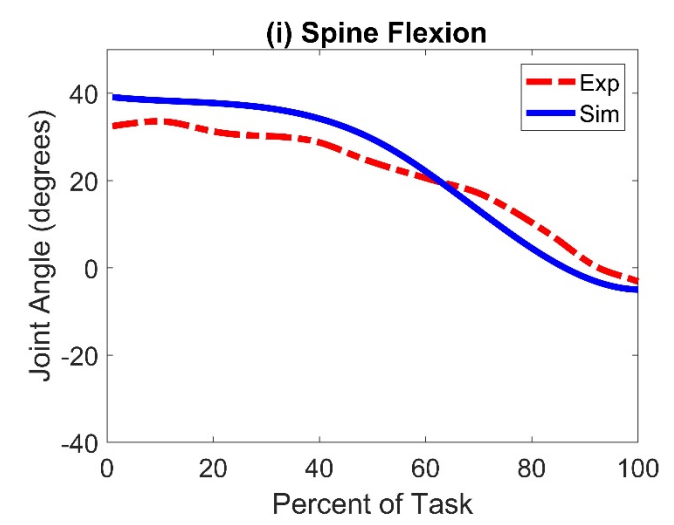


FIGURE 3: JOINT ANGLE PROFILES OF MAXIMUM WEIGHT LIFTING

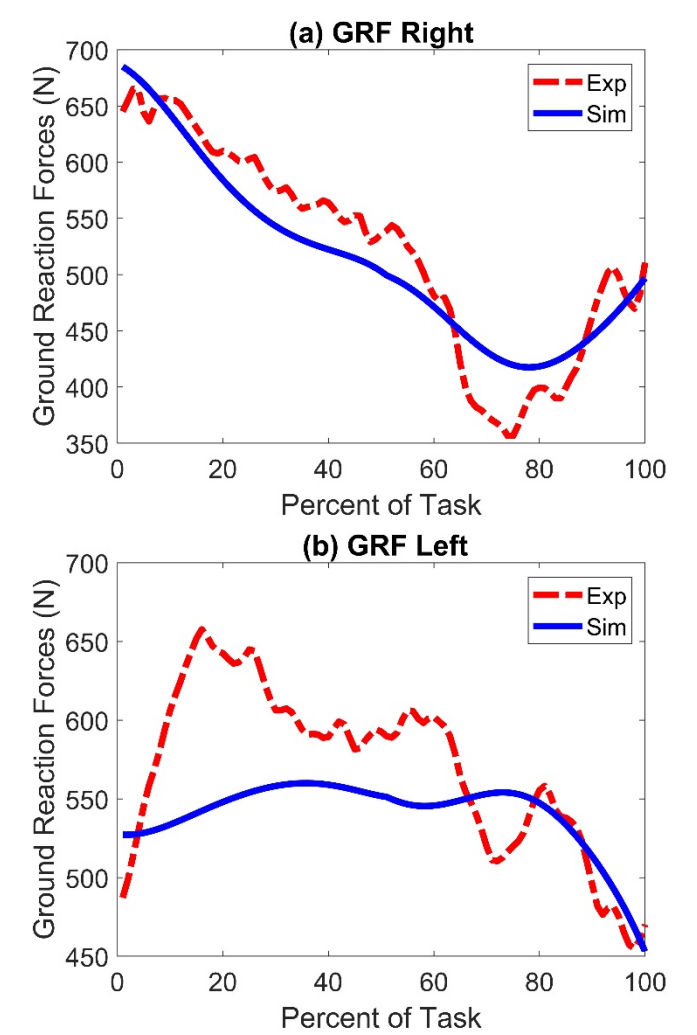


FIGURE 4: GRF PROFILES OF MAXIMUM WEIGHT LIFTING

We predicted nine important joints angles which play a vital role during symmetric lifting. The predicted joint angles agree well with the experimental data. The pattern and timing of phase changes of the predicted joint angle profiles are consistent with the experimental data. There are some minor discrepancies for the ankle joints (Figure 3a, b) and elbow joints (Figure 3g, h), but the differences are within 10 degrees. As the box weight was very heavy, the subject needed to transmit a significant amount of force through the elbow joints. The elbow (ulnohumeral joint) is mainly a hinge joint (ginglymus) and the hand side of the forearm is unsupported. Because all of these factors, it was difficult for the subject to maintain the stability during lifting heavy weight which resulted the jerking. This also made it difficult for the model to predict the elbow joints accurately.

The pattern of the predicted right vertical GRF is consistent with the experimental vertical GRF on the right side (Figure 4a). However, there are some deviations for the left GRF, particularly near 20% of the task where the difference between the GRF is more than 10% (Figure 4b). The reason of this discrepancy might be because of small initial jerks from the experimental right and left elbow angles (Figure 3a, b). The load on both hands were high above and far from the center of gravity. The small deviation of elbow angle, at the beginning of lifting, can create a significant amount of torque, which might be the reason for high peak near 20% of the task on left GRF profile. Initial jerks from the ankles (Figure 3g, h) and spine (Figure 3i) might also have contributions to such a peak in the left GRF profile. On the other hand, the predicted kinematics and kinetics curves are all smooth curves.

Note that 40 N is used as the limits for the GRF constraint Equation (20). This limit is determined based on numerical trial and error considering the convergence capability of the optimizer and robustness of the predictive model. The peak value of GRF is 650 N, so the relative error for GRF limit is 6.2%. Considering the differences between the mechanical skeletal model and real human model, this relative error for GRF limit is acceptable. Another important finding from this study is that the predicted kinetics (GRFs) are very different between left and right feet for a symmetric lifting task.

The predicted total lifting weight is 267.64 N, which is 13.5% higher than the experimental lifting weight. The reason is that the maximum lifting weight determined during the experiment is not the true maximum lifting weight. Instead, it is the maximum weight a person felt safe to lift, as mentioned in Section 3.

5. CONCLUSION

In this study, we presented a 3D skeletal model and an optimization formulation that shows good capability to accurately predict the symmetric lifting motion as well as the maximum lifting weight for a person. The lifting problem is formulated as a MOO problem by minimizing the dynamic effort and maximizing the box weight considering the dynamic joint strength. The predicted joint angle profiles and GRFs agree well with the experimental data except for some minor discrepancies for the GRF on the left foot.

One limitation of our predictive model is that, it needs some intermediate constraints to predict the lifting motion and GRFs accurately, but this is necessary for an optimization-based method to predict the joint angle profiles and GRFs accurately [18, 31, 32].

Our future work is to develop a hybrid model by combining this 3D skeletal model with OpenSim musculoskeletal model to predict and analyze muscle forces for the lifting motion [33].

ACKNOWLEDGEMENTS

This research is supported by projects from NSF (CBET 1849279 and 1703093).

REFERENCES

- [1] Murray, C. J., Lopez, A. D., and World Health Organization, 1996, The global burden of disease: a comprehensive assessment of mortality and disability from diseases, injuries, and risk factors in 1990 and projected to 2020: summary. World Health Organization.
- [2] Freburger, J.K., Holmes, G.M., Agans, R.P., Jackman, A.M., Darter, J.D., Wallace, A.S., Castel, L.D., Kalsbeek, W.D., and Carey, T. S., 2009, The rising prevalence of chronic low back pain. Archives of internal medicine, 169(3), 251-258.
- [3] Pope, M.H., Andersson, G.B., Frymoyer, J.W., and Chaffin, D.B., 1992, Occupational Low Back Pain: Assessment, Treatment, and Prevention. CRC Press.
- [4] Liberty Mutual, Liberty mutual workplace safety index, Accessed: February 2, 2020, https://business.libertymutualgroup.com/business-insurance/Documents/Services/DS200.pdf
- [5] Katz, J.N., 2006, Lumbar disc disorders and low-back pain: socioeconomic factors and consequences. The Journal of Bone and Joint Surgery, 88(suppl 2), 21-24.
- [6] Deyo, R.A., and Tsui-Wu, Y.J., 1987, Descriptive epidemiology of low-back pain and its related medical care in the United States. Spine, 12(3), 264-268.
- [7] Deyo, R.A., Cherkin, D., Conrad, D., and Volinn, E., 1991, Cost, controversy, crisis: low back pain and the health of the public. Annual Review of Public Health, 12(1), 141-156.
- [8] Zaman, R., Xiang, Y., Cruz, J., and Yang, J., 2020, Three-dimensional asymmetric maximum weight lifting prediction considering dynamic joint strength. Multibody System Dynamics (Under review).
- [9] Waters, T. R., and Garg, A., 2010, Two-dimensional biomechanical model for estimating strength of youth and adolescents for manual material handling tasks. Applied Ergonomics, 41(1), 1-7.
- [10] Chang, C.C., Brown, D.R., Bloswick, D.S., and Hsiang, S.M., 2001, Biomechanical simulation of manual lifting using spacetime optimization. Journal of Biomechanics, 34(4), 527-532.
- [11] Lin, C.J., Ayoub, M.M., and Bernard, T.M., 1999, Computer motion simulation for sagittal plane lifting activities. International Journal of Industrial Ergonomics, 24(2), 141-155.
- [12] Azghani, M.R., Farahmand, F., Meghdari, A., Vossoughi, G., and Parnianpour, M., 2009, Design and

- evaluation of a novel triaxial isometric trunk muscle strength measurement system. Proceedings of the Institution of Mechanical Engineers, Part H: Journal of Engineering in Medicine, 223(6), 755-766.
- [13] Frey-Law, L. A., Laake, A., Avin, K.G., Heitsman, J., Marler, T., and Abdel-Malek, K., 2012, Knee and elbow 3D strength surfaces: peak torque-angle-velocity relationships. Journal of Applied Biomechanics, 28(6), 726-737.
- [14] Hussain, S.J., and Frey-Law, L., 2016, 3D strength surfaces for ankle plantar-and dorsi-flexion in healthy adults: an isometric and isokinetic dynamometry study. Journal of Foot and Ankle Research, 9(1), 43.
- [15] Looft, J.M., 2014, Adaptation and validation of an analytical localized muscle fatigue model for workplace tasks, Ph.D. thesis, Department of Biomedical Engineering, The University of Iowa, Iowa City, IA.
- [16] Gundogdu, O., Anderson, K. S., and Parnianpour, M., 2005, Simulation of manual materials handling: Biomechanial assessment under different lifting conditions. Technology and Health Care-European Society for Engineering and Medicine, 13(1), 57-66.
- [17] Xiang, Y., Zaman, R., Rakshit, R., and Yang, J., 2019, Subject-specific strength percentile determination for two-dimensional symmetric lifting considering dynamic joint strength. Multibody System Dynamics, 46(1), 63-76.
- [18] Xiang, Y., Cruz, J., Zaman, R., and Yang, J., 2020, Multi-objective optimization for two-dimensional maximum weight lifting prediction considering dynamic strength. Engineering Optimization, (in press).
- [19] Sreenivasa, M., Millard, M., Kingma, I., Van Dieen, J. H., and Mombaur, K., 2018, Predicting the influence of hip and lumbar flexibility on lifting motions using optimal control. Journal of biomechanics, 78, 118-125.
- [20] Song, J., Qu, X., and Chen, C. H., 2016, Simulation of lifting motions using a novel multi-objective optimization approach. International Journal of Industrial Ergonomics, 53, 37-47.
- [21] Xiang, Y., Rahmatalla, S., Chung, H. J., Kim, J., Bhatt, R., Mathai, A., Beck, S., Marler, T., Yang, J., Arora, J.S., Abdel-Malek, K., and Obusek, J., 2008, Optimization-based dynamic human lifting prediction (No. 2008-01-1930). SAE Technical Paper.
- [22] Xiang, Y., Arora, J. S., and Abdel-Malek, K., 2012, 3D human lifting motion prediction with different performance measures. International Journal of Humanoid Robotics, 9(02), 1250012.
- [23] Xiang, Y., Arora, J. S., Rahmatalla, S., Marler, T., Bhatt, R., and Abdel-Malek, K., 2010, Human lifting simulation using a multi-objective optimization approach. Multibody System Dynamics, 23(4), 431-451.
- [24] Xiang, Y., Arora, J. S., and Abdel-Malek, K., 2012, Hybrid predictive dynamics: a new approach to simulate human motion. Multibody System Dynamics, 28(3), 199-224.
- [25] Rana, G.M., 2018, Maximum weight lifting prediction considering dynamic joint strength. Master thesis, Department of

- Mechanical Engineering, University of Alaska Fairbanks, AK, USA.
- [26] Hartenberg, R.S., and Denavit, J., 1955, A kinematic notation for lower pair mechanisms based on matrices.
- [27] Xiang, Y., Arora, J. S., and Abdel-Malek, K., 2009, Optimization-based motion prediction of mechanical systems: sensitivity analysis. Structural and Multidisciplinary Optimization, 37(6), 595-608.
- [28] Vukobratović, M., and Borovac, B., 2004, Zeromoment point—thirty five years of its life. International Journal of Humanoid Robotics, 1(01), 157-173.
- [29] Xiang, Y., Arora, J. S., Rahmatalla, S., and Abdel-Malek, K., 2009, Optimization-based dynamic human walking prediction: One step formulation. International Journal for Numerical Methods in Engineering, 79(6), 667-695.
- [30] Gill, P.E., Murray, W., and Saunders, M.A., 2005, SNOPT: An SQP algorithm for large-scale constrained optimization. SIAM review, 47(1), 99-131.
- [31] Chung, H.J., Xiang, Y., Mathai, A., Rahmatalla, S., Kim, J., Marler, T., Beck, S., Yang, J., Arora, J.S., Abdel-Malek, K., Obusek, J., 2007, A robust formulation for prediction of human running. SAE Technical Paper, 2007-01-2490.
- [32] Rakshit, R., Xiang, Y., Yang, J., 2020, Dynamic-joint-strength-based two-dimensional symmetric maximum-weight lifting simulation: Model development and validation. Journal of Engineering in Medicine, (in press).
- [33] Zaman, R., Xiang, Y., Rakshit, R., and Yang, J., 2019, Muscle force prediction in OpenSim using skeleton motion optimization results as input data. ASME 2019 International Design Engineering Technical Conferences and Computers and Information in Engineering Conference. August 18–21, Anaheim, California, USA.